4050 *Macromolecules* **2010**, *43*, 4050–4061
DOI: 10.1021/ma1001904

Macromolecules
ARTICLE

Peptide−Polymer Bioconjugates via Atom Transfer Radical Polymerization and Their Solution Aggregation into Hybrid Micro/Nanospheres for Dye Uptake

Tapas K. Paira, Sanjib Banerjee, Manoj Raula, Atanu Kotal, Satyabrata Si, and Tarun K. Mandal*

Polymer Science Unit, Indian Association for the Cultivation of Science, Jadavpur, Kolkata 700 032, India

Received January 25, 2010; Revised Manuscript Received April 7, 2010

ABSTRACT: Peptide−polymer hybrid bioconjugates containing poly(methyl methacrylate) chains attached with oligopeptide molecules were prepared by atom transfer radical polymerization (ATRP) using designed peptide-initiators. These initiators were synthesized from newly designed peptides with 2-bromoisobutyric acid via a standard coupling reaction. ATRP of methyl methacrylate was conducted using Br-terminated peptide as macroinitiator and copper(I) chloride/*N*,*N*,*N*′,*N*″,*N*″-pentamethyldiethylenetriamine as the catalyst system in dimethyl sulfoxide (DMSO) at an elevated temperature (90 °C). The peptide−polymer bioconjugates with controllable molecular weights and low polydispersities (PDI < 1.35) were obtained. We devised a simple solution approach in assembling the peptide−polymer bioconjugate molecules into hybrid micro/nanospheres in different organic solvents as confirmed from transmission electron microscopy (TEM), field emission scanning electron microscopy (FESEM), and dynamic light scattering (DLS) results. The average size of the formed hybrid micro/nanospheres decreases with the increase of the polarity of the solvent used in aggregation process. A mechanistic model was suggested for the aggregation of peptide−polymer conjugates into hybrid micro/nanospheres that correlates well with the experimental observation. The dye-loaded hybrid micro/nanospheres were simply prepared by mixing an organic dye (Rhodamine 6G) into the aggregated solution of peptide−polymer bioconjugates. The uptake of dye into the micro/nanospheres was studied by fluorescence microscopy and time-correlated single photon counting (TCSPC) techniques.

Introduction

Peptide−polymer hybrid bioconjugates are currently receiving a great deal of attention from the polymer and materials science community due to their wide applications in the field of biotechnology,[1] medicine,[2,3] and in biomedical applications.[4] The covalent attachment of the polymer to the peptides or proteins offers a number of advantages. For example, a protein or peptide block may control the nanostructure formation of the synthetic component,[5−7] whereas a synthetic polymer block may increase the stability[8] by preventing the enzymatic degradation or unfolding of protein/peptide segment that also increases the biocompatibility of the same polymer segment.[9,10] Consequently, researchers have designed a variety of bioactive nanomaterials by utilizing these kinds of hybrids.[11,12] Some of these hybrid bioconjugates can also self-organize into hydrogels through the interaction of their peptide/protein component, which can be used in drug delivery and in tissue engineering.[11,13]

In recent years, there have been various polymerization techniques for synthesizing these types of peptide−polymer hybrids in a well-controlled manner.[14,15] However, atom transfer radical polymerization (ATRP)[16,17] has proved to be the very powerful and easy technique among all the living polymerization techniques[18] to synthesize such kinds of conjugates. A survey of the literature shows that peptide−polymer hybrids have been usually synthesized mainly by two different approaches. In the first approach, polymer with controlled molecular weight and well-defined functionality at the chain end were first synthesized using available controlled radical polymerization (CRP) techniques. The as-synthesized polymer with predefined functionality was then coupled (through its chain end) with amino acid or peptide or protein side chain using the simple coupling chemistry.[19−22] The second approach is a two-step process consisting of the modification of peptide or protein with initiators followed by the polymerization of appropriate monomer using these modified macroinitiator by different controlled polymerization techniques.[23−30]

By applying these two basic approaches, researchers have prepared several different types of peptide−polymer hybrids consisting of peptides of varying sequences as well as polymers of different monomers. There were also some other methods for the preparation of such hybrids that are based on the modification of the above-mentioned two basic approaches. For example, Borner and co-workers synthesized different peptide−polymer hybrids by ATRP[28] and RAFT[31] of different monomers using oligopeptide-based initiators containing either 2-bromopropionate or dithioester moiety, respectively. Biesalski and co-workers synthesized peptide−polymer conjugates by a combination of self-assembling functional cyclic peptides and in situ surface-initiated ATRP.[32] Wooley et al. have used valine-based ATRP initiator to polymerize *tert*-butyl acrylate and chain extended with styrene to produce polymers and diblock copolymer with amino acid functionality.[29] Biohybrid materials containing polystyrene and polymethacrylates have also been prepared by using amino acid ATRP initiators.[33]

Recently, there have been several reports on the use of so-called bottom-up approaches to prepare organic/bioorganic nanostructured materials. Among these approaches, the

*Corresponding author: Fax 91-33-2473 2805, e-mail psutkm@mahendra.iacs.res.in.

 Published on Web 04/15/2010

Scheme 1. Synthesis of Peptide-Initiators and Peptide−Polymer Hybrid Conjugates[a]

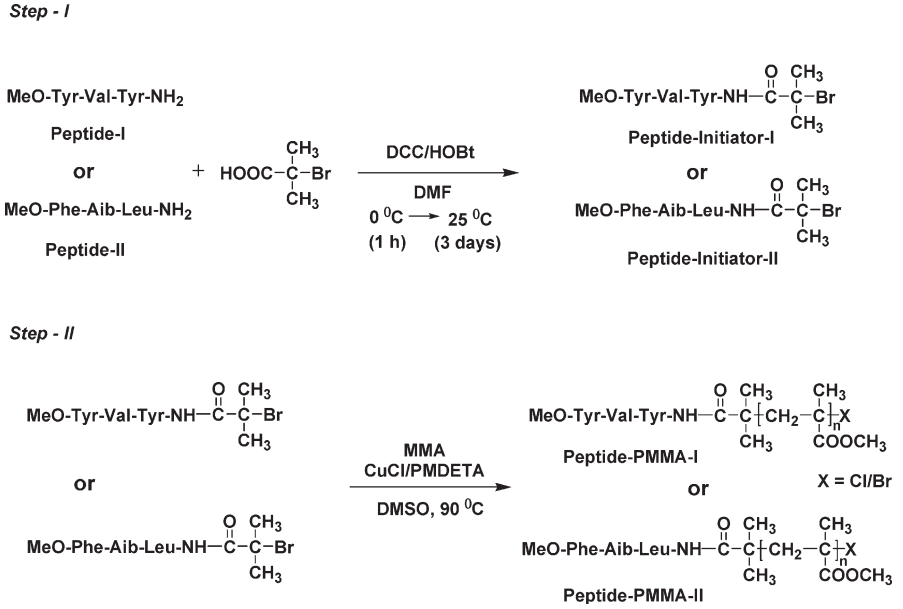

[a] DCC = dicyclohexylcabodiimide; HOBt = 1-hydroxybenzotriazole; DMF = dimethylformamide; MMA = methyl methacrylate; PMDETA = *N*,*N*,*N*′,*N*″,*N*″-pentamethyldiethylenetriamine.

self-organization/aggregation of peptide−polymer hybrid molecules into different nanostructured materials in different solvents is noticeable. In these cases, the peptide segment of the hybrid molecule generally assembled through different supramolecular interaction and directed the shape of the nanostructures formed through the assembly process. Nanostructured hybrid materials with varieties of shapes such as nanotube,[19,32,34] nanoribbon,[35] vesicles,[36] nanosphere,[37] and helical[20] have been prepared from different peptide−polymer conjugates by their assemblies in solution. Although, most of such assemblies have been carried out in aqueous environment[32,34] and in mixed solvent,[36,38] but the use of single organic solvent as medium for such assemblies is limited.[39,40]

In the present study, we wish to report the successful synthesis of peptide−poly(methyl methacrylate) (peptide−PMMA) hybrid bioconjugates by ATRP using newly designed peptide-based initiators (see Scheme 1). We investigated the kinetics of formation as well as the evolution of molecular weight and molecular weight distributions (MWD) of the obtained peptide−PMMA bioconjugates. The as-prepared peptide−PMMA conjugate molecules were then aggregated into different-sized hybrid micro/nanospheres in different polar organic solvents (acetonitrile, dimethyl sulfoxide, and dimethylformamide). We incorporated a representative dye (Rhodamine 6G) into these hybrid micro/nanospheres to prepare dye-loaded micro/nanospheres. We also studied the dye uptake via fluorescence microscopic and time-resolved fluorescence spectroscopic techniques. This study helps to somewhat better understand this aggregation of peptide−polymer conjugate molecules into spherelike hybrid micro/nanostructures.

Experimental Section

Materials. L-Valine (Val), L-tyrosine (Tyr), L-leucine (Leu), α-aminoisoburyric acid (Aib), L-phenylalanine (Phe), dicyclohexylcarbodiimide (DCC), 1-hydroxybenzotriazole (HOBt), and di-*tert*-butylpolycarbonate (Boc) were purchased from SRL India. 2-Bromoisobutyric acid, Rhodamine 6G, copper(I) chloride (CuCl) (purity >98%), and *N*,*N*,*N*′,*N*″,*N*″-pentamethyldiethylenetriamine (PMDETA) (purity >99%) were purchased from Aldrich and were used without further purification. CuCl was also purified by according to the literature procedure.[41] Methyl methacrylate (MMA) (Burgoyne Urbridges and Co.) was washed with 5% (w/v) of aqueous NaOH solution to remove all the inhibitors, dried with calcium chloride overnight, and distilled over calcium hydride under reduced pressure prior to use in the polymerization reaction. Dimethyl sulfoxide (DMSO) and dimethylformamide (DMF) (Merck, India) were distilled over calcium hydride under reduced pressure just before use. Thionyl chloride ($SOCl_2$) was distilled twice before use in the reaction. All other solvents (Merck, India) were used as received.

Synthesis of Peptides. The synthesis of peptide-I [NH_2-Tyr(1)-Val(2)-Tyr(3)-OMe] and peptide-II [NH_2-Leu(1)-Aib(2)-Phe(3)-OMe] involves first the preparation of the N-protected peptide-I [Boc-Tyr(1)-Val(2)-Tyr(3)-OMe] and N-protected peptide-II [Boc- Leu(1)-Aib(2)-Phe(3)-OMe] followed by deprotection with formic acid. The latter two N-protected peptides were synthesized by conventional solution phase methods using racemization-free fragmentation/condensation strategy. The Boc group was used for N-terminal protection and the C-terminus was protected as a methyl ester. Couplings were mediated by dicyclohexylcarbodiimide/1-hydroxybenzotriazole (DCC/HOBt). All intermediates were characterized by ^{1}H NMR spectroscopy (300 MHz) and thin-layer chromatography (TLC) on silica gel and used without further purification.

Synthesis of N-Protected Peptide-1 [Boc-Tyr(1)-Val(2)-Tyr(3)-OMe]. The N-protected peptide-1 was prepared by following our earlier reported method.[42] Typically, a sample of Boc-Tyr(1)-Val(2)-OH (3.64 g, 10 mmol) (for synthesis see the Supporting Information) in DMF was cooled and kept in an ice−water bath. The methyl ester of tyrosine (H_2N-Tyr-OMe) (3.9 g, 20 mmol) (see Supporting Information for synthesis) was then added to this solution. Finally, DCC (2.06 g, 10 mmol) and HOBt (1.35 g, 10 mmol) were added to the above reaction mixture. The reaction mixture was stirred for 3 days in a magnetic stirrer. The resultant product was taken in ethyl acetate (30 mL), and DCU was filtered off. The organic layer was washed with HCl (2 N, 3 × 20 mL), brine (1 × 20 mL), sodium carbonate (1 M, 3 × 20 mL), and brine (2 × 20 mL). The organic layer was then dried over anhydrous sodium sulfate and evaporated under vacuum. Purification was carried out by silica gel column chromatography (100−200 mesh) by using ethyl acetate/toluene as the eluent (see Supporting Information for NMR and ESI mass data).

Synthesis of N-Protected Peptide-II [Boc-Leu(1)-Aib(2)-Phe(3)-OMe]. The N-protected peptide-II was similarly synthesized following the above-mentioned procedure that used for N-protected peptide-I (see Supporting Information for NMR and ESI mass data).

Synthesis of Peptide-I [NH_2-Tyr(1)-Val(2)-Tyr(3)-OMe]. For deprotection of Boc group, 10 mL of formic acid (98%) was added to Boc-Tyr(1)-Val(2)-Tyr(3)-OMe (2.78 g, 5 mmol), and the subsequent removal of the Boc group was monitored via TLC. After 6 h of reaction, the formic acid was removed under vacuum. The residue containing peptide-I (see Figure S1 for chemical structure) was then dissolved in water (40 mL) and washed with diethyl ether (2 × 30 mL). The pH of the aqueous solution was adjusted to 8 with sodium bicarbonate, and the peptide-I was extracted with ethyl acetate (3 × 20 mL). The organic extracts were collected, washed with saturated brine, dried over sodium sulfate, and evaporated under reduced pressure to obtained purified peptide-I (see Supporting Information for NMR and ESI mass data).

Synthesis of Peptide-II [NH_2-Leu(1)-Aib(2)-Phe(3)-OMe]. Similarly, peptide-II (see Figure S1 for structure) was also obtained by deprotecting the Boc group of N-protected peptide-II following the above-mentioned procedure as used for the synthesis of peptide-I (see Supporting Information for NMR and ESI mass data).

Synthesis of Peptide-Initiator-I [$Me_2C(Br)$-CO-NH-Tyr(1)-Val(2)-Tyr(3)-OMe]. The peptide-initiator-I was synthesized from peptide-1 with 2-bromoisobutyric acid via a standard coupling procedure using DCC/HOBT as the coupling agent (see Scheme 1). Briefly, a sample of 2-bromoisobutyric acid (0.417 g, 2.5 mmol) in DMF (20 mL) was cooled in an ice−water bath. Peptide-I (1.37 g, 3 mmol) was then added to this solution. Next, DCC (0.515 g, 2.5 mmol) and HOBt (0.405 g, 3 mmol) were simultaneously added to the above reaction mixture. The reaction mixture was stirred for 3 days with a magnetic stirrer. After completion of the reaction, ethyl acetate (30 mL) was added to the final mixture and the precipitated DCU was filtered off. The organic layer was washed with HCl (2 N, 3 × 20 mL), brine (1 × 20 mL), sodium carbonate (1 M, 3 × 20 mL), and brine (2 × 20 mL). The organic layer containing peptide-initiator-I was then dried over anhydrous sodium sulfate and evaporated under vacuum. Further purification of peptide-initiator-I was done via silica gel column chromatography (100−200 mesh) using a mixture of ethyl acetate/toluene as the eluent. Yield = 1.28 g (2.12 mmol, 85%). ^{1}H NMR (300 MHz, d_6-DMSO, TMS) (see Figure S2): δ = 9.20 and 9.11 (s, 2H, tyrosinate proton), 8.40−8.38 (d, 1H, J = 6.72 Hz, −NH), 7.98−7.96 (d, 1H, J = 8.08 Hz, −NH), 7.65−7.62 (d, 1H, J = 8.73 Hz), 7.01−6.96 (d, 4H, J = 8.1 Hz, Tyr (1)/Tyr (3) ring hydrogen), 6.65−6.57 (d, 4H, J = 8.1 Hz, Tyr (1)/Tyr (3) ring hydrogen), 4.41−4.32 (m, 2H, C^{α}−H of Tyr (1) and Tyr (3)), 4.25−4.20 (m, 1H, C^{α}−H of valine), 3.52 (s, 3H, $-OCH_3$), 2.91−2.76 (m, 4H, C^{β}−H of Tyr (1) and Tyr (3)), 1.94−1.90 (m, 1H, C^{β}−H of valine), 1.75 (s, 6H, C^{β}−H of 2-bromoisobutyric acid), 0.84−0.79 ppm (d, 6H, C^{γ}−H of valine). MS (ESI) (35 eV): m/z (%): 628 (100) [M + Na^+] (see Figure S4).

Synthesis of Peptide-Initiator-II [$Me_2C(Br)$-CO-NH-Leu(1)-Aib(2)-Phe(3)-OMe]. Peptide-initiator-II was synthesized following the above-mentioned procedure as used for the synthesis of peptide-initiator-I. Yield = 1.05 g (2 mmol, 80%). ^{1}H NMR (300 MHz, $CDCl_3$, TMS) (see Figure S3): δ = 7.27−7.24 and 7.12−7.09 (m, 5H, aromatic ring proton), 6.91−6.89 (d, 1H, J = 7.5 Hz, −NH), 6.78−6.75 (d, 1H, J = 7.68 Hz, −NH), 6.59 (s, 1H, −NH), 4.84−4.78 (m, 1H, C^{α}−H of Leu(1)), 4.31−4.24 (m, 1H, C^{α}−H of Phe(3)), 3.70 (s, 3H, $-OCH_3$), 3.18−3.04 (m, 2H, C^{β}−H of Leu(1)), 1.94 and 1.92 (s, 6H, C^{β}−H of 2-bromoisobutyrate), 1.47 and 1.43 (s, 6H, C^{β}−H of Aib(2)), 0.97−0.92 ppm (d, 6H, C^{γ}−H of valine). MS (ESI) (35 eV): m/z (%): 550 (100) [M + Na^+] (see Figure S5).

Synthesis of Peptide−Poly(methyl methacrylate) (Peptide−PMMA) Hybrid Bioconjugates. In a typical polymerization procedure, 0.04 g (0.067 mmol) of peptide-initiator-I and 0.0065 g (0.067 mmol) of CuCl were taken in a 25 mL long neck round-bottom flask, which was then fitted with a high-temperature rubber septum. The flask was purged with nitrogen for 10 min. DMSO and MMA monomer was deoxygenated separately by purging with nitrogen for 30 min. 4 mL of deoxygenated DMSO and 1.5 mL of MMA were added to the above reaction mixture via syringe, and nitrogen gas was purged for further 20 min. 11 μL (0.067 mmol) of PMDETA was then injected to the reaction mixture, and the reaction flask was placed in a preheated oil bath at constant temperature of 90 °C. Aliquots (1.5 mL) were taken from the reaction mixture time to time via a syringe for determining conversion and molecular weight by GPC analysis. The resultant peptide−PMMA hybrid conjugate was isolated by dilution of the aliquots with methanol. We designated this hybrid as peptide−PMMA-I. The precipitated hybrid was isolated by centrifugation, washed repeatedly with methanol, and finally dried in a vacuum oven at 60 °C. The monomer conversion was determined by gravimetric analysis of the isolated and dried hybrid. For NMR and GPC analysis, the isolated hybrid was further dissolved in THF, and the dilute THF solution was passed through neutral alumina column to remove any traces of catalyst impurities therein. Finally, the purified hybrid polymers were isolated by precipitating in methanol.

Similarly, peptide-initiator-II was also used to prepare hybrid conjugates and was designated as peptide−PMMA-II. This hybrid contains peptide with different sequence than that present in peptide−PMMA-I hybrid mentioned above.

Aggregation Procedure. For aggregation study, typically, the as-synthesized and purified peptide−PMMA conjugate (5 mg) was dissolved in different solvent such as CH_3CN, DMF, and DMSO and was kept for 7 days in a closed vial. The aggregation of peptide−polymer conjugate into hybrid micro/nanospheres was monitored by field emission scanning electron microscopy (FESEM), transmission electron microscopy (TEM), and dynamic light scattering (DLS). The time evolution of size of the hybrid micro/nanospheres growing in the solution of peptide−polymer conjugates was also studied via DLS.

Dye Uptake Procedure. For dye uptake study, 5 mg of an as-synthesized peptide−PMMA hybrid was added to the 1 mL of 10^{-5} M Rhodamine 6G (R6G) solution of DMF and allowed to stand for 7 days. To ensure total saturation of uptake of dye to the as-formed hybrid spheres, we kept the system undisturbed for such a long time. This solution was then added dropwise into excess water under shaking for better dispersion of the hybrid spheres. Finally, hybrid polymeric spheres containing the incorporated dye, R6G, were isolated by centrifugation. The precipitate (isolated micro/nanospheres) was further washed 10 times by centrifugation to remove any physically adsorbed R6G dye on the surface of the spheres. The dye-loaded hybrid micro/nanospheres were dispersed in DMF and were subjected to analysis using fluorescence microscopy and time-correlated single photon counting (TCSPC) technique.

Characterization. *NMR Experiments*. For ^{1}H NMR studies, all the peptides and peptide-initiators were dissolved in either $CDCl_3$ or d_6-DMSO, and peptide−PMMA hybrid was dissolved in $CDCl_3$. ^{1}H NMR spectra were acquired in a Bruker DPX 300 MHz spectrometer.

ESI Mass Spectrometry. The ESI mass spectra of the as-synthesized peptides and peptide-initiators were recorded from their methanol solution in a quadrupole time-of-flight (Qtof) Micro YA263 mass spectrometer.

GPC Measurement. Molecular weights and molecular weight distributions of the synthesized peptide−polymer conjugates were measured by size exclusion chromatography (SEC) using a Waters 1515 isocratic HPLC pump connected to three Waters Styragel HR1, HR3, and HR4 columns and a Waters 2414 refractive index detector at room temperature (25 °C). The effective molecular weight separation ranges of these columns

are 100−5000, 500−30 000, and 5000−500 000, respectively. THF was used as eluent with a flow rate of 1 mL/min, and narrow polystyrene standards having peak molecular weights (M_p) 3600, 8500, 19 100, 43 400, 76 300, and 139 400 were used for calibrating the GPC. Waters Breeze Software was used for molecular weight analysis.

FESEM Measurement. Peptide−PMMA hybrids and neat PMMA were first dissolved in different organic solvents, drop-cast on small pieces of glass, and allowed the film to dry overnight in air. The piece of glass containing the sample was then mounted on a SEM holder followed by platinum coating to make it conducting. All SEM images were taken in a JEOL field emission scanning electron microscope (model JSM-6700F) operating at an accelerating voltage of 5 kV.

DLS Measurement. All DLS experiments were carried out on a Brookhaven Instruments photon correlation spectrometer equipped with a Bl-200SM research goniometer system, a TurboCorr digital correlator, and a He−Ne laser (632.8 nm). Measurements were made at 25 °C. We used distilled and filtered acetonitrile, dimethylformamide, and dimethyl sulfoxide as solvent to dissolve hybrids. For all cases, 5 mg of a peptide−PMMA hybrid was dissolved in 2 mL of organic solvent (e.g., CH_3CN, DMF, and DMSO) and filtered through a membrane filter (0.45 μm pore size). DLS measurements of these filtered solutions were then carried out at different time intervals.

TEM Measurement. For transmission electron microscopic measurements, the samples were prepared by drop-casting the dilute suspension of the hybrid spheres onto a carbon-coated Cu grid followed by drying in air. The images were then recorded on a JEOL JEM-2010 electron microscope operated at an accelerating voltage of 100 kV.

Fluorescence Microscopic Measurement. For acquiring fluorescence microscopic images of the dye-encapsulated aggregated peptide−PMMA hybrid spheres, the following method was used. A small quantity of dye-encapsulated hybrid sphere was dispersed in DMF, and the suspension was placed on a glass slide and images were recorded. Fluorescence microscopy was conducted using a light microscope (BX61, Olympus) equipped with a filter set consisting of a BP530−550 nm for an exciter and a band absorbance filter covering wavelengths below 420 nm.

Time-Correlated Single-Photon Counting (TCSPC) Measurements. Time-resolved fluorescence spectra of the dye (R6G)-loaded hybrid micro/nanospheres were acquired by the TCSPC technique using a picosecond diode laser (IBH Nanoled-07) in an IBH Fluorocube apparatus. A suspension of dye-loaded micro/nanospheres was first excited at 440 nm. The typical full width at half-maximum (fwhm) of the system response using a liquid scatter is about 110 ps. The fluorescence decay of R6G present inside the hybrid spheres was collected with a Hamamatsu MCP photomultiplier (C487802) and was analyzed using IBH DAS6 software. For comparison, the fluorescence decay of neat R6G in DMF was also collected and analyzed.

Results and Discussion

Synthesis of Peptide−Polymer Hybrid Bioconjugates. The synthesis of peptide−PMMA hybrid bioconjugates involved the following steps: (1) the preparation of tripeptides (peptide-I and peptide-II, for chemical structures see Figure S1); (2) the attachment of an ATRP initiator (2-bromoisobutyric acid) to the N-terminus of these as-synthesized tripeptides to produce peptide-based initiators (peptide-initiator-I and peptide-initiator-II; for their chemical structures see Figure S1) (for synthesis see step I of Scheme 1); (3) the polymerization of methyl methacrylate (MMA) by ATRP using these peptide-based initiators as macroinitiators in DMSO at an elevated temperature (90 °C) (see step II of Scheme 1).

We have chosen the above-mentioned model oligopeptide for making peptide−polymer hybrids conjugates. It has been reported that these classes of oligopeptide molecules can undergo self-assembly into nanostrucutred materials of different shapes such as nanotube, nanosphere, etc., through various types of noncovalent interactions.[43,44] Therefore, by attaching a synthetic polymer chain with such peptide, we expect that we would be able to prepare these types of nanostructured materials, which would be made up of hybrid materials containing peptide and polymer. These peptides were prepared by following our earlier reported method of conventional solution phase synthesis by using a racemization−free fragmentation/condensation strategy.[42,45]

The free N-terminus of the as-synthesized peptides (peptide-I and peptide-II) were then coupled with an ATRP initiator, 2-bromoisobutyric acid, using DCC/HOBT as the coupling agent (see step I of Scheme 1) to obtain the desired peptide-initiators (peptide-initiator-I or peptide-initiator-II). The yield of this coupling reaction was ~80%. The ^{1}H NMR spectrum of the purified peptide-initiator-I (see Figure S2) showing a peak at $\delta = 1.75$ ppm corresponds to the protons of two methyl groups of the ATRP initiator, 2-bromoisobutyrate moiety, along with all the other characteristics peaks corresponding to other functional groups present in the peptide-I moiety. Similarly, the ^{1}H NMR spectrum of the purified peptide-initiator-II (see Figure S3) shows both the characteristic peaks of the two methyl groups of 2-bromoisobutyric acid and peptide-II. The integral intensity of methyl protons of ATRP initiator moieties (see H_i in Figure S2) was almost equal with that of C^{γ}-protons of valine group of the peptide-I moiety (see H_m in Figure S2), showing the purity of the peptide-initiator-I. Similarly, for peptide-initiator-II, the integral intensity of methyl protons of ATRP initiator moieties (see H_i in Figure S3) was almost equal to that of C^{δ}-protons of leucine (see H_m in Figure S3) of the peptide-II. The ESI-mass spectra (see Figures S4 and S5) of peptide-initiator-I and peptide-initiator-II show respective molecular ion peaks at m/z 628 $(M_{\text{peptide-initiator-I}} + Na)^+$ and 550 $(M_{\text{peptide-initiator-II}} + Na)^+$, respectively. Thus, these results are indicative of successful introduction of the ATRP initiator (2-bromoisobutyric acid) to one end of these peptide chains with the above-mentioned sequences.

These peptide-initiators were then utilized for conducting an ATRP of MMA monomer. However, these peptide-initiators were insoluble in most of the common ATRP solvents such as toluene, xylene, anisole, etc., but are soluble in dipolar aprotic solvent such as DMSO. Therefore, DMSO was chosen as the solvent for conducting the ATRP of MMA using these initiators at 90 °C using CuCl/PMDETA as the catalyst system with a molar ratio of 1:1.

In order to study the kinetics of the above-mentioned polymerization system initiated with peptide-initiator-I, known aliquots were taken out at different time intervals, and the monomer conversion was measured gravimetrically (see Experimental Section for details). Figure 1A shows the semilogarithmic plot of the monomer concentration vs time. It is clear that the plot is not linear throughout the whole time period of the reaction, rather a slightly curved one, which indicates that this polymerization as a whole does not follow first-order kinetics.

However, the data during an initial period (within 30 min of polymerization time) of this plot show a linear time dependency. This result reveals that the reaction followed the first-order kinetics up to monomer-to-polymer conversion of about 23%. Although, first-order kinetics cannot be claimed until over 90% conversion has been reached. But, there are reports where first-order kinetics was claimed at as low as 15% conversion[46] and 60% conversion[47] in the ATRP of butyl acrylate (BA) and 2-hydroxyethyl methacrylate

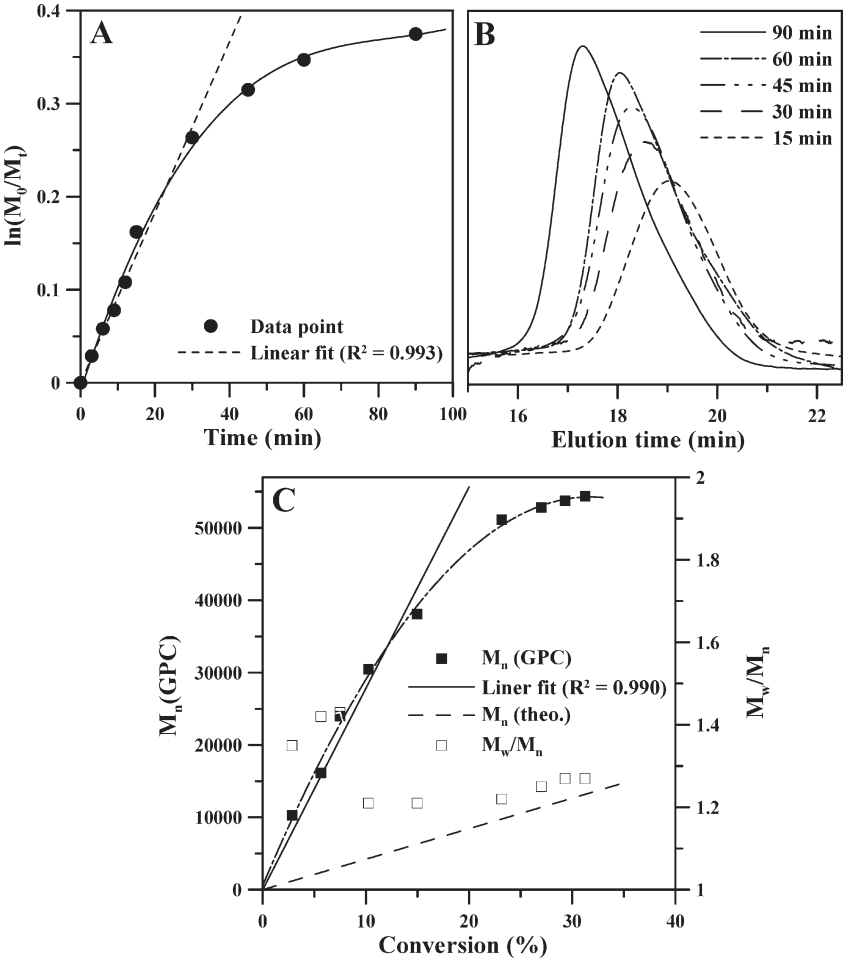

Figure 1. Polymerization of MMA by ATRP initiated by peptide-initiator-I in the presence of catalyst CuCl/PMDETA in DMSO at 90 °C: (A) semilogarithmic plot of monomer concentration vs time; (B) GPC traces of hybrids obtained at different time intervals; (C) dependence of M_n and PDIs of obtained hybrids with conversion. Conditions: $[MMA]_0/[\text{peptide-initiator-I}]_0/[CuCl]_0/[PMDETA]_0 = 421:1:1:1$.

(HEMA), respectively. Therefore, this polymerization is well controlled up to this conversion (~23%). But, it is expected that this polymerization reaction should follow first-order rate kinetics throughout the whole conversion range, since it has been reported that the initiator (2-bromoisobutyric acid) that is attached with the peptide has been used alone as a successful ATRP initiator for the polymerization MMA using CuBr/*N*-(*n*-butyl)-2-pyridylmethanimine[48] catalyst systems, and this polymerization followed perfectly first-order kinetics up to a very high polymerization conversion.

The deviation from the linearity in the semilogarithmic plot arises may be due to the progressive decrease in the actual catalyst concentration throughout the polymerization process as also reported by other researchers for their systems.[28] In this case, the decrement of the catalyst concentration is probably due to the decrease in the concentration of complex of CuCl/PMDETA as part of the initially added CuCl form a new complex with peptide moiety of the initiator molecule probably through its amide functional group. To prove this supposition that the peptide moiety formed complex with CuCl during the polymerization reaction, we carried out a control experiment. In this experiment, MMA was polymerized using CuCl/BOC-Tyr-Val-Tyr-OMe instead of CuCl/PMDETA as a catalyst and ethyl-2-bromo-isobutyrate as an initiator in the molar ratio of 1:1:1 in DMSO at 90 °C for 36 h. In this case, indeed we observed the formation of PMMA, but the monomer-to-polymer conversion was only ~20%. The low reactivity of the used catalyst system might be responsible for such low monomer-to-polymer conversion. However, the GPC traces of the obtained PMMA are unimodal in nature (see Figure S6), indicating that the reaction proceeded through a well-controlled manner.

Another control experiment was also carried out to show further the effect of amide functional group of peptide in the kinetics of this polymerization reaction. A model tyrosine-based initiator (Tyr-initiator) was synthesized (see page S4 of for synthesis and Figure S7 for ^{1}H NMR spectrum in the Supporting Information). The ATRP of MMA was then carried out using this Tyr-initiator and CuCl/PMDETA as catalyst systems in DMSO at 90 °C. The semilogarithmic plot of the monomer-to-polymer concentration vs time of this polymerization system also deviates from linearity (see Figure S8). In this context, to check whether the tyrosine phenol group of the initiator has any role for retardation or inhibition of this polymerization, we synthesized a phenylalanine-based model initiator (Phe-initiator) where the phenolic group is absent (see page S5 of for synthesis and Figure S9 for ^{1}H NMR spectrum in the Supporting Information). This initiator was then used to carry out the polymerization of MMA under similar reaction conditions [catalyst: CuCl/PMDETA; solvent: DMSO; temperature = 90 °C] as used in the cases of peptide-initiator-I and Tyr-initiator. The first-order kinetic plot of the MMA/Phe-initiator polymerization system was also not linear and was similar to that of the MMA/Tyr-initiator system (see Figure S8). However, the rate of polymerization is negligibly higher when Phe-initiator

Table 1. Polymerization Conditions and the Molecular Characterization Data of the Peptide−Polymer Hybrid Bioconjugates Prepared by Varying the Molar Ratios of Monomer to Initiator[a]

sample	$[M]_0/[I]_0$	time (h)	conv (%)	$M_{n,theo}$ (kDa)	$M_{n,GPC}$ (kDa)	PDI (M_w/M_n)
peptide−PMMA-Ia	100	36	55	5.50	24.9	1.20
peptide−PMMA-Ib	200	36	50	10.0	33.0	1.25
peptide−PMMA-Ic	220	36	50	11.0	41.0	1.26
peptide−PMMA-Id	350	36	50	17.5	51.6	1.21
peptide−PMMA-Ie	500	36	50	25.0	62.5	1.30
peptide−PMMA-If	680	36	50	34.0	75.4	1.35
peptide−PMMA-IIa	110	64	72	7.90	19.4	1.50
peptide−PMMA-IIb	350	64	70	24.5	60.0	1.29

[a] Conditions: $[I]_0$ = [peptide-initiator-I or peptide- initiator-II]$_0$ = 1.98×10^{-5} M; solvent = DMSO; temperature = 90 °C. Peptide−PMMA-(Ia-If) = polymer prepared with peptide-initiator-I. Peptide−PMMA-(IIa-IIb) = polymer prepared with peptide-initiator-II.

was used instead of Tyr-initiator (see Figure S10). For example, for Tyr-initiator the yield was ~26% in 75 min, whereas for Phe-initiator the yield was ~35% in 75 min. From these results, one could say that the effect of tyrosine phenol group of initiator on this polymerization is very little. On the other hand, it has been reported that the ATRP of MMA using ester derivative of 2-bromoisobutyric acid (ethyl 2-bromoisobutyrate) as initiator and CuBr/PMDETA as catalyst follows perfectly first-order kinetics.[49] Thus, it can be concluded that the presence of amide functional group in the Tyr-initiator/Phe-initiator as well as in the peptide-initiator-I is mainly responsible for such discrepancy in kinetics. Teodorescu et al. have also observed nonlinearity in the first-order kinetic plot for the ATRP of amide-functionalized monomer (methacrylamide) using CuBr/Me_4Cyclam[50] and CuCl/Me_6TREN[51] as catalyst systems. They also mentioned that the nonlinearity of the semilogarithmic plot in their system was due to inactivation of catalyst because of complexation of CuCl with polyacrylamide as well as the parent monomer during the polymerization reaction. Rettig et al. have also found such nonlinearity in the ATRP of *n*-butyl acrylates in DMSO using a peptide-initiator and CuBr/PMDETA as catalyst systems.[28] The details of this type of interaction between CuCl and peptide moiety of our initiator and their effect on the kinetics of ATRP of MMA are under investigation.

One reviewer suggested whether the impurity present in CuCl might be responsible for the sluggishness of the polymerization reaction. To examine this, we performed the ATRP of MMA using the purified CuCl (purified according to a procedure reported elsewhere[41]) and keeping all other reaction parameters similar as used for peptide−PMMA-Ia hybrid (see Table 1). After 36 h of polymerization, the yield of the polymer was found to be ~55%, which is almost the same (55%, see Table 1) as obtained using CuCl of 98% purity. The M_n and PDI of the obtained PMMA (at 36 h) were 30.5 kDa and 1.28, respectively (see Figure S11), which are very similar to those of peptide−PMMA-Ia obtained using CuCl (purity 98%). These results indicated that the purity of CuCl is not responsible for the sluggishness or the low conversion of the polymerization reaction.

The molecular weight (M_n) and molar mass distribution (MWDs) of the obtained peptide−PMMA-I hybrids were measured by GPC using THF as the eluent. The GPC traces of hybrids obtained at different time interval are provided in the Figure 1B. The traces exhibit a continuous shifting toward lower retention time, indicating the increment of the molecular weight of the respective hybrids with time. The traces (see Figure 1B) were unimodal in nature, clearly indicating that the polymerization proceeded in a controlled manner. Figure 1C shows the plot of M_n and the polydispersities (PDI = M_w/M_n) of the obtained peptide−PMMA-I hybrids as a function monomer-to-polymer conversion in the polymerization system initiated with peptide−initiator-I.

The plot clearly shows that the M_n of the hybrids increases linearly with increasing conversion, but up to a conversion of ~20%. This is indicative to the controlled nature of this polymerization. However, after this point of conversion, there is a clear deviation with a very slow increase of the M_n with conversion (see Figure 1C). Similar deviation was also observed in the semilogarithmic plot of the monomer concentration vs time as mentioned above (see Figure 1A). Although, in each case, the measured molecular weights (M_ns) are always higher than the theoretical M_ns. Also, the PDIs of the obtained hybrids remained narrow and decreased slowly with increasing monomer conversion (up to ~20%), as expected from a controlled polymerization. However, after this conversion, the PDI increased slowly. This result indicated the presence of some termination reaction.

Peptide−PMMA-I hybrids with different molecular weights are readily accessible by changing the initial monomer-to-initiator ratio ($[M]_0/[I]_0$) (see Table 1). Hybrids (peptide−PMMA-Ia to peptide−PMMA-If) of different molecular weights ranging from 25 to 75 kDa with PDIs of 1.20 to 1.35 (see Table 1) were synthesized from a peptide-initiator-I simply by changing monomer-to-initiator ratio. Similarly, different hybrids (peptide−PMMA-IIa and peptide−PMMA-IIb) were also synthesized using peptide-initiator-II (see Table 1). Table 1 clearly indicates that experimental M_ns are always higher than the theoretically calculated M_ns. A similar observation was also reported by many researchers when amide-functionalized initiators were used in the ATRP of different monomers. Earlier researchers have also observed a similar discrepancy in the experimental and theoretical M_n values when polymerization was carried out using amide-functionalized initiator[46] and some kind of oligopeptide-based initiators in DMSO.[52]

The attachment of a peptide moiety to one end of a PMMA chain was confirmed via ^{1}H NMR characterization of one of the representative purified hybrids: peptide−PMMA-Ia. This sample was purified several times by dissolving in THF and precipitating in methanol. The spectrum of this sample clearly exhibits two signals at δ = 7.06 and 6.80 ppm (see Figure 2), which could be assigned to the ring proton of tyrosine moiety of peptide-I. The rest of other signals corresponding to the peptide-initiator-I were merged with PMMA signals, and therefore, we would not be able to identify those signals. But the presence of tyrosine residue certainly confirmed that the peptide-I moiety is attached at the end of PMMA chain of the hybrid peptide−PMMA.

Self-Aggregation of Peptide−Polymer Hybrid Bioconjugates. It has been reported that the peptide−polymer hybrid molecules have a great tendency toward aggregation in different solvents or cosolvents mainly due to the amphiphilic nature of the hybrids or the interactions (e.g., H-bonding, π-stacking ability, hydrophobic) presents in the peptide or in the polymer part.[32,34,36,37] Therefore, we are interested in exploring the aggregation behavior of the as-synthesized peptide−PMMA hybrids in different organic solvents. For this study, we first dissolved a representative hybrid (peptide−PMMA-Ia, see Table 1) in different solvents such as CH_3CN, DMF, and DMSO. The concentration of the hybrid was 5 mg/mL for each solvent. The solutions were equilibrated for several days (depending on the solvent used) in a closed vessel.

Figure 3 shows the FESEM images of the obtained nanostructures formed by the aggregation of peptide−PMMA-Ia

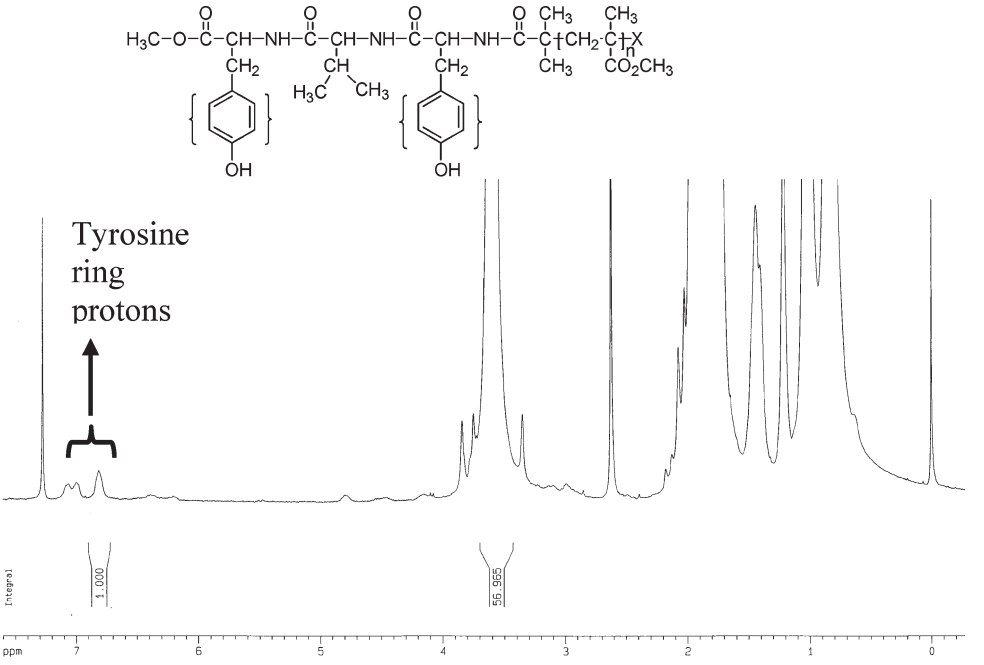

Figure 2. ^{1}H NMR spectrum of peptide−PMMA-Ia in $CDCl_3$.

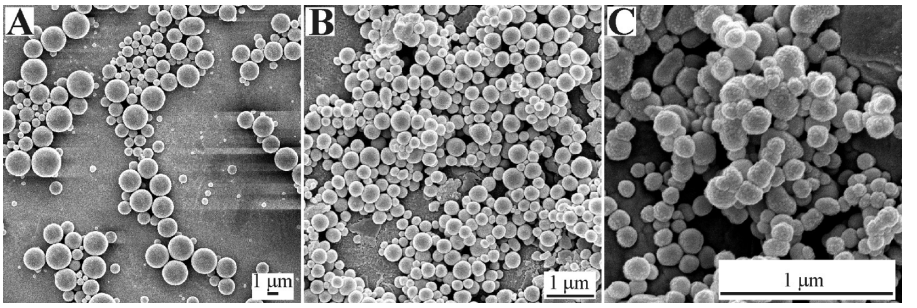

Figure 3. FESEM images of hybrid micro/nanospheres obtained by aggregation of a representative hybrid (peptide−PMMA-Ia) in different organic solvents: (A) CH_3CN, (B) DMF, and (C) DMSO.

hybrid molecules in different solvents. These images clearly show that the hybrid molecules are aggregated into discrete, tiny spheres in all of the above-mentioned solvents. Judging from these images, it seems that the average diameter of the spheres depends on the solvent polarity. For this, we determined the diameter of 100 spheres obtained from CH_3CN as shown in Figure 3A and found spheres of mainly three types of size distributions. These are 14% spheres within range of 250−500 nm, 38% spheres within range of 500−1000 nm, and 48% spheres within the range of 1500−2200 nm. These results reveal that the polydispersity of the obtained aggregated spheres is very high. However, in DMF (Figure 3B) and in DMSO (Figure 3C), the hybrid molecules are mostly aggregated into nanospheres. The diameters of the nanospheres obtained from DMF are in the range of 150−470 nm. A histogram analysis of the size distribution of the obtained nanospheres in this case is provided in Figure S12. Interestingly, the average sizes of the aggregated hybrid nanospheres obtained from DMSO are much smaller than that of nanospheres obtained from DMF and especially that of micro/nanospheres obtained from CH_3CN. The diameters of these spheres are in the range of 75−180 nm. Figure S13 shows the histogram analysis of the particle size distribution of the spheres obtained from DMSO solution. Thus, it can be concluded that the average sizes of the formed hybrid micro/nanospheres depended on the polarity of the solvent used in aggregation process.

To check whether there is any effect of molecular weight of the hybrid on the size and shape of formed aggregated nanostructures, we performed the aggregation experiment using different peptide−PMMA hybrids of varying M_n in DMF. Figures S14A−C show the FESEM images of the aggregated nanostructures obtained from different hybrid samples, peptide−PMMA-Ia, peptide−PMMA-Ib, and peptide−PMMA-If in DMF, respectively (see Table 1). It can be seen from these images that the aggregated nanostructures obtained from these hybrids are mostly spherical in shape. However, the high molecular weight hybrid (sample peptide−PMMA-If) molecules are aggregated into some oblong-shaped particles along with the as usual spherical-shaped particles. The average sizes of the aggregated spheres obtained from samples peptide−PMMA-Ia, peptide−PMMA-Ib, and peptide−PMMA-If are in the ranges of 150−470, 365−610, and 280−550 nm, respectively, as measured form these images (see Figures S14(A−C), respectively). Thus, we may conclude that there is no appreciable change in size of the spheres obtained by the aggregation of the hybrids of varying molecular weights.

We also study the aggregation of peptide−PMMA-II conjugate molecules, whose peptide sequence is different

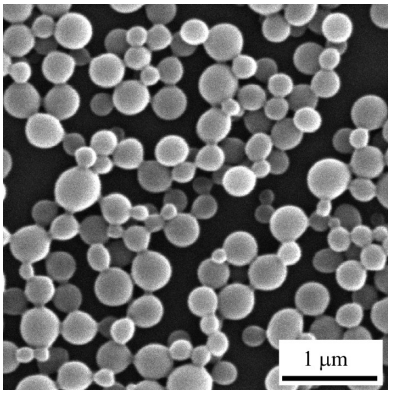

Figure 4. FESEM image of hybrid nanospheres obtained by the aggregation of peptide−PMMA-IIa in DMF.

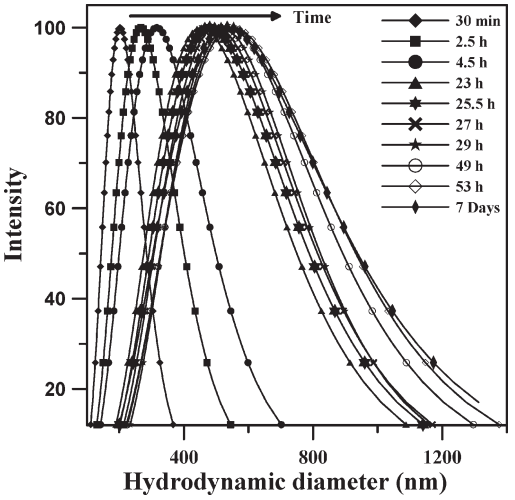

Figure 5. Plot showing log-normal distributions of the sizes of the spherical aggregated peptide−PMMA-Ia hybrid (0.5 wt %) in CH_3CN with their hydrodynamic diameters at different time.

from that of peptide−PMMA-I molecule (see Scheme 1 for structures of the hybrids), in DMF to examine whether there is any effect of the peptide sequence on the shape and size of the formed nanostructures. Figure 4 shows the FESEM image of the nanostructures obtained by the aggregation of one of such representative hybrid, peptide−PMMA-IIa (see Table 1) in DMF. The image also shows the formation of nanospheres having diameter in the range of 200−500 nm.

In order to provide further support that hybrid micro/nanospheres are formed by the aggregation of peptide−polymer hybrid molecules in solution, TEM measurements were performed for peptide−PMMA-Ia hybrid in CH_3CN, by placing one drop of the solution onto a carbon-coated copper grid. The TEM image (see Figure S15) showed the formation of spheres with diameters in the ranges of 500−1000 nm and 1−2.3 μm. Therefore, it can be concluded that the TEM results correlates well with results of FESEM investigations (see Figure 3A) of acetonitrile.

To understand this aggregation process of peptide−polymer conjugates and to ascertain the nature of the aggregated structures obtained through this aggregation process in solution, we performed the DLS measurements of 0.5 wt % solution of a representative hybrid (peptide−PMMA-Ia, M_n = 24.9 kDa; see Table 1) in different solvents such as CH_3CN, DMF, and DMSO. We were able to monitor the size evaluation of the aggregated hybrid spheres in CH_3CN. The representative log-normal distributions of

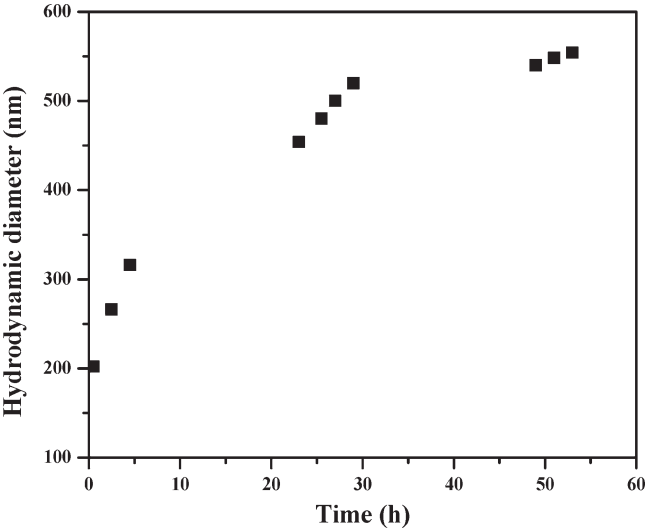

Figure 6. Plots showing the variation of hydrodynamic diameters of the spheres obtained from peptide−PMMA-Ia (0.5 wt %) hybrid in CH_3CN against time. Hydrodynamic diameters were obtained from log-normal size distributions shown in Figure 5.

the sizes of the obtained hybrid spheres with the increase in time are plotted in Figure 5. From Figure 5, it is clear that the hydrodynamic diameter of the hybrid spheres increases as the time progresses.

The hydrodynamic diameters of the hybrid spheres are plotted against time in Figure 6 which clearly shows a consistent increase in the size of the aggregated spheres with time. This result also indicates that the size of the obtained spheres reaches almost its saturation after 53 h (~2.5 days) of aggregation, which indicates that the aggregation process is dynamic in nature. The non-negatively constrained least-squares (NNLS) distribution of the hybrid spheres obtained from CH_3CN after 30 min (see Figure S16) showed spheres of mainly two types of size distribution in the range of 6−12 and 174−323 nm with equal intensity. But, after 7 days, hybrid spheres of three types of size distributions (4−12, 150−450, and 550−1300 nm with higher intensity) were obtained (see Figure S17).

Furthermore, it should be noted that the population of smaller sized particles (4−12 nm) diminishes whereas the number and the diameter of the large size spheres increase as time elapsed (compare Figures S16 and S17 in the Supporting Information). This result may indicate that the large size spheres are formed by the aggregation of small size spheres, the details of which will be discussed later in this section.

The log-normal distributions of the sizes of the hybrid spheres obtained from DMF and DMSO after 7 days are shown in the Figure 7. These distributions indicate that the hydrodynamic diameters of the hybrid spheres obtained from DMF and DMSO are 404 and 100 nm, respectively. These results are consistent with that obtained from FESEM results (see Figure 3B,C). From the DLS results, we may conclude that the hybrid spheres are formed by the self-aggregation of peptide−polymer conjugate molecules in solution.

For better understanding of the aggregation process, we carried out some control experiments. For this, the neat peptide-I (NH_2-Tyr-Val-Tyr-OMe) and the neat polymers (PMMA) were dissolved in CH_3CN at a concentration of 0.5 wt % and kept them for 7 days for aggregation. Note that the neat PMMA (M_n = 25 000) was synthesized by ATRP of MMA using ethyl 2-bromoisobutyrate initiator following the procedure described elsewhere.[53] Interestingly, we found

that the neat peptide-I molecule assembled into spherical particles with an average size is around 550−1300 nm (see Figure 8A). However, as mentioned above, the average size of the hybrid peptide−PMMA spheres obtained from CH_3CN range from 250 to 2200 nm. Thus, it can be concluded that there is no appreciable change in size of neat peptide spheres due to hybrid formation. But, both the neat peptide and peptide−polymer hybrid were assembled into spherical particles. But, we did not observe the formation of any such spheres due to the aggregation of neat PMMA molecules (see Figure 8B). It has also been reported that oligopeptides can assemble into several different shaped nanostructures other than spheres.[34] The formations of these micro/nanostructures are guided primarily through peptides due to the presence of various noncovalent interactions between peptide molecules. Thus, it is our thought that the peptide moieties present in our conjugates are mainly

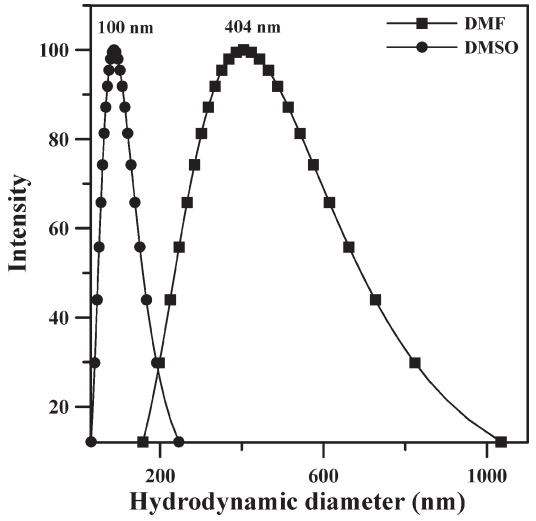

Figure 7. Plot showing log-normal distributions of the sizes of the spherical aggregated peptide−PMMA-Ia hybrid (0.5 wt %) in DMF and DMSO with their hydrodynamic diameters.

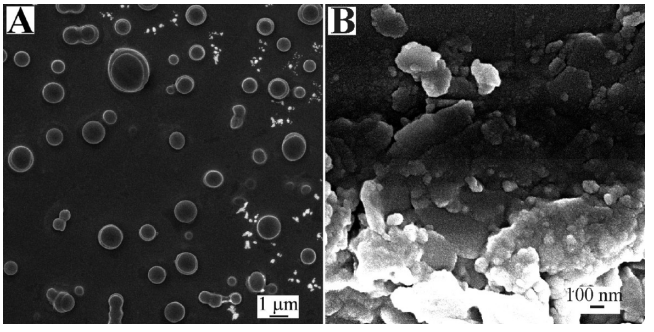

Figure 8. FESEM images of (A) self-assembled neat peptide-I and (B) aggregated neat PMMA in CH_3CN.

responsible for the formation of such hybrid micro/nanospheres. It is worth mentioning that this self-aggregation process largely depends on the polarity of the solvents. For example, the aggregation of hybrid molecules in THF and $CHCl_3$ did not result in the formation of any micro/nanospheres.

On the basis of above-mentioned DLS results, results of the control experiments, and the literature reports, we can propose the following mechanistic model for the formation hybrid micro/nanospheres in this case. Our bioconjugate molecule consists of two parts: (a) the peptide part (Tyr-Val-Tyr) and (b) the polymer (PMMA) part. The used solvents (CH_3CN, DMF, and DMSO) are actually good solvents for the peptide part but are not very good for the PMMA part. Thus, when peptide−polymer conjugate molecules are dissolved in any one of the above-mentioned solvents, it would be expected that initially micelles would formed in the solution, where the more soluble peptide part exists in the outer part of the micelle facing the solvent directly and the PMMA part in the core as shown schematically shown in Scheme 2. In fact, as mentioned above, we indentified small particles of around 4−12 nm size via DLS when 0.5 wt % solution of peptide−PMMA-Ia was kept in CH_3CN for 30 min (see Figure S16) along with the particles of sizes in the range of 174−323 nm. We believe that these small particles are the initially formed small micelles. However, we did not find such small particles via FESEM and TEM. The formation of such small block copolymer micelles in a single solvent (organic/water) is well reported in the literature.[39,40,54−57] Among these reports, Zhang and Eisenberg have found that the poly(styrene-*block*-acrylic acid) and poly(styrene-*block*-ethyl oxide) were assembled into micro/nanospheres in aqueous solution. They were the first to explain that the micro/nanospheres are actually the large compound micelles formed by the secondary aggregation of primary micelles.[57,58] The formation of large micelle named as supermicelle has also been reported by Muller et al.[54,55] Later on, it has been reported that the hyperbranched star copolymers were self-assembled into large multimolecular complex micelle in water through similar secondary aggregation mechanism.[56] Thus, we believe that a similar kind of mechanism is also operating in our case. That is, the initially formed small micelles, as mentioned above, undergo secondary aggregation to form large size composite micelles, as shown in Scheme 2. We believe that these composite micelles are the micro/nanospheres as observed through FESEM and TEM mentioned above, which are composed of initially formed small peptide−polymer micelles. This aggregation of small spheres/particles (micelles) into large composite micelles (micro/nanospheres) is also evident from DLS results (mentioned above), which shows that the sizes of the spheres increase with time (see Figures 5 and 6). DLS data also showed the population of smaller sized particles (micelles) (4−12 nm) diminishes whereas the number and the diameter of the large size spheres (composite micelles) increase with time (compare Figures S16 and S17 in the

Scheme 2

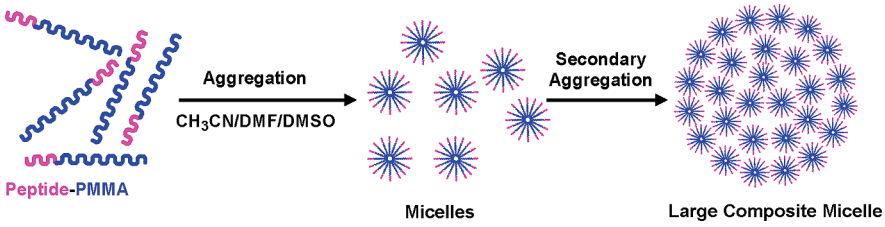

Supporting Information). This result also supports the secondary aggregation mechanism. The H-bonding and $\pi-\pi$ interactions between the peptide moieties might be responsible for such secondary aggregation.

Dye Uptake Study. Finally, we are interested in preparing dye-loaded hybrid micro/nanospheres. It is our expectation that the study of incorporation of a dye into the aggregated micro/nanospheres provides us better understanding of this aggregation process. For this, the aggregation of the peptide–PMAA-Ia hybrids was carried out in the presence of the Rhodamine 6G (R6G) dye in DMF. After 7 days, one drop of this solution was examined via a fluorescence microscope, and the images of the dye-loaded aggregated hybrid micro/nanospheres are provided in Figure 9A. For comparison purposes, the DMF solution of R6G without hybrids was also examined via a fluorescence microscope, and we did not observe any sphere formation in this case as no hybrids were present in this case (see Figure 9B). Upon comparison of these images (Figure 9A,B), it is very clear that R6G molecules nicely encapsulated/incorporated into the aggregated micro/nanospheres during the aggregation process. Hardly any bare R6G molecules remain in the DMF solution as the background of the Figure 9A did not show any signal of dye molecule. A cartoon presentation is given in Scheme 3 for better visualization of the process of dye incorporation into the hybrid micro/nanosphere during the aggregation of peptide–polymer conjugates in DMF.

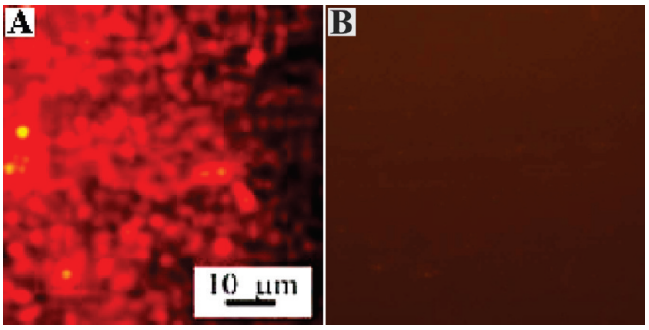

Figure 9. Fluorescent light microscopy images of (A) Rhodamine 6G incorporated aggregated peptide–PMMA-Ia hybrid micro/nanospheres and (B) neat Rhodamine 6G in DMF.

Scheme 3. Cartoon Representation of the Dye Incorporation into the Micro/Nanospheres during the Aggregation of Peptide–PMMA Hybrid Conjugates in DMF

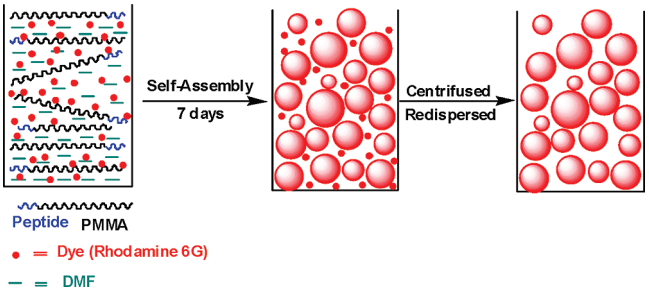

To know whether the dye molecules are actually incorporated into the aggregated spheres or it is just simply adsorbed on the surface of such spheres, we performed the time-resolved fluorescence study of the R6G-loaded hybrid spheres dispersed in DMF using the TCSPC technique. For comparison, we also performed the time-resolved fluorescence study of the bare R6G molecules in DMF solution. The time-resolved fluorescence data (fluorescence decay curves) of bare R6G and the R6G incorporated into spheres were fitted with the equation

$$I(t) = \sum_{i=1}^{N} A_i \exp(-t/\tau_i) \quad (1)$$

Here, A_i and τ_i are the relative amplitude and lifetime of the ith fluorescence component, respectively. N is the number of the fluorescence exponentials required for best nonlinear least squares (NLLS) fitting of the fluorescence decay curves. The fluorescence decay curves for the bare R6G and incorporated R6G into sphere are represented in Figure 10.

When fitted with the eq 1, the bare R6G gave single-exponential decay with the time scale of 3.38 ns (see Figure 10A and Table 2 for details), whereas the incorporated R6G showed biexponential decay as shown in Figure 10B. The time scales were 3.38 ns with relative amplitude of 0.85 and 6.67 ns with relative amplitude of 0.15 (see Table 2). The 3.38 ns time scale is the lifetime of R6G in DMF. In the case of incorporated R6G dye, the origin of slower component (6.67 ns) is probably the result of restricted motions (mainly

Table 2. Nonlinear Least Squares (NLLS) Fitting Parameters Obtained from the Fluorescence Decay Curves (Given in Figure 10) using Eq 1 for Bare R6G and R6G Incorporated into Micro/Nanospheres in DMF

sample	A_1	τ_1 (ns)	A_2	τ_2 (ns)	χ^2
bare R6G	1	3.38			1.06
R6G incorporated spheres	0.85	3.38	0.15	6.67	1.15

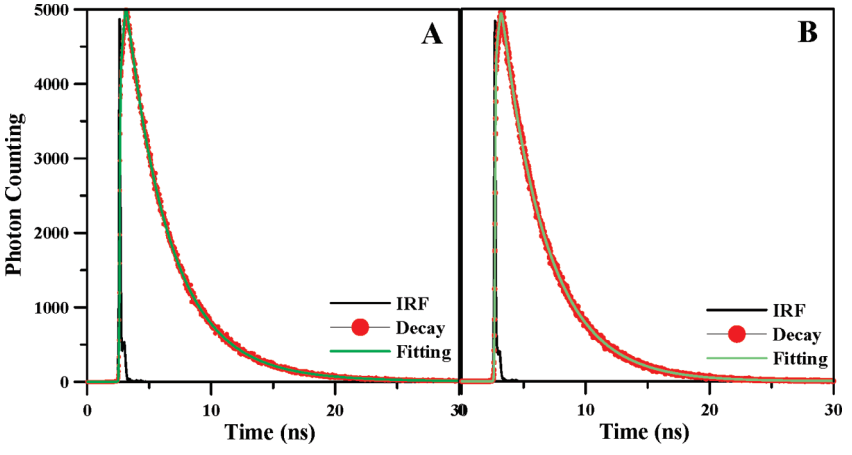

Figure 10. Time-dependent decay curves of Rhodamine 6G in DMF: (A) bare R6G; (B) R6G incorporated into hybrid micro/nanospheres.

translational) of the R6G dye molecules due to its incorporation into the nanospheres of the hybrid molecules during aggregation. This result indicates that R6G dye molecules are well entrapped into the formed hybrid nanospheres by the aggregation of the peptide−PMMA hybrids in DMF. As R6G is a dipolar molecule, therefore, one could easily expect that this dye molecule can interact with the amide linkages of the peptide moiety through dipole−dipole interactions. The aggregation of the peptide−PMMA may be due to the interaction of the amide linkages present in the peptide unit and the hydrophobic interaction of the polymer units.

Conclusions

Peptide−polymer hybrid bioconjugates of varying molecular weights and peptide sequences were prepared by the ATRP of MMA using different newly designed peptide-initiators and CuCl/PMDETA as the catalyst system in DMSO at 90 °C. Control of this polymerization process up to a certain stage of reaction was confirmed by kinetic studies of the MMA polymerization using peptide-based initiators that were synthesized by the coupling reaction of different peptides with 2-bromoisobutyric acids by conventional solution phase method. The unimodal nature of the GPC traces of the hybrids indicated that the polymerizations were well controlled, producing peptide−polymer hybrids with controlled molecular weights and low polydispersities (PDI < 1.35). A probable explanation was given for getting nonlinear kinetics plot and higher molecular weight polymer than the theoretical values of this system. The peptide−PMMA conjugate molecules aggregated into micro/nanospheres in different organic solvents as confirmed from TEM, FESEM, and DLS results. The average sizes of the obtained hybrid spheres decrease with the increase of the polarity of the solvent used in the aggregation process. It appears that the peptide−polymer conjugate molecules first aggregated to form small micelles that eventually further combined through secondary aggregation process to form large size composite micelles (micro/nanospheres). We demonstrated as a proof of concept that an organic dye (Rhodamine 6G) can easily be incorporated inside the as formed hybrid micro/nanospheres by mixing it into the aggregated solution to prepare dye-loaded spheres. Time-resolved fluorescence study and fluorescence microscopy study confirmed the dye incorporation into the hybrid spheres. These dye-loaded micro/nanospheres could be used in various applications including paints and coatings. These hybrid spheres have the potential to be used as micro/nanocarriers for drug delivery.

Acknowledgment. T.K.P., S.B., and M.R. thank CSIR, India, for the fellowship. This research was supported by the grants from CSIR, India. Thanks are also due to the partial support from the Nanoscience and Nanotechnology Initiatives, DST, India.

Supporting Information Available: Synthesis procedure of small peptide sequence and tyrosine-based model initiator (Tyr-initiator), NMR, and ESI-mass data of peptides, ^{1}H NMR spectra of peptide-initiator-I, peptide-initiator-II, model Tyr-initiator and Phe-initiator, ESI-mass spectra of peptide-initiator-I and peptide-initiator-II, GPC trace of PMMA using CuCl/Boc-Tyr-Val-Tyr-OMe as catalyst, kinetics of polymerization using model Tyr-initiator and Phe-initiator, histogram analysis of particle size distribution (from FESEM images) of the aggregated micro/nanospheres obtained from peptide-PMMA-Ia in DMF and DMSO, histogram of NNLS distribution for pep-PMMA-Ia in CH_3CN. This material is available free of charge via Internet at http://pubs.acs.org.

References and Notes

(1) Tirrell, J. G.; Fournier, M. J.; Mason, T. L.; Tirrell, D. A. *Chem. Eng. News* **1994**, *72*, 40–51.
(2) Duncan, R. *Nat. Rev. Drug Discovery* **2003**, *2*, 347–360.
(3) Bae, Y.; Fukushima, S.; Harada, A.; Kataoka, K. *Angew. Chem., Int. Ed.* **2003**, *42*, 4640–4643.
(4) Harris, T. J.; von Maltzahn, G.; Lord, M. E.; Park, J.-H.; Agrawal, A.; Min, D. H.; Sailor, M. J.; Bhatia, S. N. *Small* **2008**, *4*, 1307–1312.
(5) Pechar, M.; Kopeckova, P.; Joss, L.; Kopecek, J. *Macromol. Biosci.* **2002**, *2*, 199–206.
(6) Hentschel, J.; Krause, E.; Borner, H. G. *J. Am. Chem. Soc.* **2006**, *128*, 7722–7723.
(7) Eckhardt, D.; Groenewolt, M.; Krause, E.; Borner, H. G. *Chem. Commun.* **2005**, 2814–2816.
(8) Hamley, I. W.; Ansari, I. A.; Castelletto, V.; Nuhn, H.; Rosler, A.; Klok, H.-A. *Biomacromolecules* **2005**, *6*, 1310–1315.
(9) Harris, J. M.; Chess, R. B. *Nat. Rev. Drug Discovery* **2003**, *2*, 214–221.
(10) Vandermeulen, G. W. M.; Klok, H.-A. *Macromol. Biosci.* **2004**, *4*, 383–398.
(11) Elemans, J. A. A. W.; Rowan, A. E.; Nolte, R. J. M. *J. Mater. Chem.* **2003**, *13*, 2661–2670.
(12) Kim, J. K.; Anderson, J.; Jun, H. W.; Repka, M. A.; Jo, S. *Mol. Pharmaceutics* **2009**, *6*, 978–985.
(13) Klok, H.-A. *J. Polym. Sci., Part A: Polym. Chem.* **2005**, *43*, 1–17.
(14) Hentschel, J.; Bleek, K.; Ernst, O.; Lutz, J.-F.; Borner, H. G. *Macromolecules* **2008**, *41*, 1073–1075.
(15) Becker, M. L.; Liu, J.; Wooley, K. L. *Chem. Commun.* **2003**, 180–181.
(16) Matyjaszewski, K.; Xia, J. *Chem. Rev.* **2001**, *101*, 2921–2990.
(17) Pintauer, T.; Matyjaszewski, K. *Chem. Soc. Rev.* **2008**, *37*, 1087–1097.
(18) Zhang, K.; Li, H.; Zhao, S.; Wang, W.; Wang, S.; Xu, Y.; Yu, W.; Wang, J. *Polym. Bull.* **2006**, *57*, 253–259.
(19) ten Cate, M. G. J.; Severin, N.; Borner, H. G. *Macromolecules* **2006**, *39*, 7831–7838.
(20) Hentschel, J.; Borner, H. G. *J. Am. Chem. Soc.* **2006**, *128*, 14142–14149.
(21) Burkoth, T. S.; Benzinger, T. L. S.; Urban, V.; Lynn, D. G.; Meredith, S. C.; Thiyagarajan, P. *J. Am. Chem. Soc.* **1999**, *121*, 7429–7430.
(22) Rosler, A.; Klok, H.-A.; Hamley, I. W.; Castelletto, V.; Mykhaylyk, O. O. *Biomacromolecules* **2003**, *4*, 859–863.
(23) Bontempo, D.; Li, R. C.; Ly, T.; Brubaker, C. E.; Maynard, H. D. *Chem. Commun.* **2005**, 4702–4704.
(24) Bontempo, D.; Maynard, H. D. *J. Am. Chem. Soc.* **2005**, *127*, 6508–6509.
(25) Heredia, K. L.; Tolstyka, Z. P.; Maynard, H. D. *Macromolecules* **2007**, *40*, 4772–4779.
(26) Lele, B. S.; Murata, H.; Matyjaszewski, K.; Russell, A. J. *Biomacromolecules* **2005**, *6*, 3380–3387.
(27) Qi, K.; Ma, Q.; Remsen, E. E.; Clark, J. C. G.; Wooley, K. L. *J. Am. Chem. Soc.* **2004**, *126*, 6599–6607.
(28) Rettig, H.; Krause, E.; Borner, H. G. *Macromol. Rapid Commun.* **2004**, *25*, 1251–1256.
(29) Venkataraman, S.; Wooley, K. L. *Macromolecules* **2006**, *39*, 9661–9664.
(30) Zeng, Q.; Li, T.; Cash, B.; Li, S.; Xie, F.; Wang, Q. *Chem. Commun.* **2007**, 1453–1455.
(31) ten Cate, M. G. J.; Rettig, H.; Bernhardt, K.; Borner, H. G. *Macromolecules* **2005**, *38*, 10643–10649.
(32) Couet, J.; Biesalski, M. *Macromolecules* **2006**, *39*, 7258–7268.
(33) Broyer, R. M.; Quaker, G. M.; Maynard, H. D. *J. Am. Chem. Soc.* **2008**, *130*, 1041–1047.
(34) Couet, J.; Jeyaprakash, J. D.; Samuel, S.; Kopyshev, A.; Santer, S.; Biesalski, M. *Angew. Chem., Int. Ed.* **2005**, *44*, 3297–3301.
(35) Collier, J. H.; Messersmith, P. B. *Adv. Mater.* **2004**, *16*, 907–910.
(36) Ayres, L.; Hans, P.; Adams, J.; Lowik, D. W. P. M.; van Hest, J. C. M. *J. Polym. Sci., Part A: Polym. Chem.* **2005**, *43*, 6355–6366.
(37) Waku, T.; Matsusaki, M.; Kaneko, T.; Akashi, M. *Macromolecules* **2007**, *40*, 6385–6392.
(38) Adams, D. J.; Atkins, D.; Cooper, A. I.; Furzeland, S.; Trewin, A.; Young, l. *Biomacromolecules* **2008**, *9*, 2997–3003.
(39) Tung, P.-H.; Kuo, S.-W.; Chen, S.-C.; Lin, C.-L.; Chang, F.-C. *Polymer* **2007**, *48*, 3192–3200.
(40) Jenekhe, S. A.; Chen, X. L. *Science* **1999**, *283*, 372–375.
(41) Keller, R. N.; Wycoff, H. D. *Inorg. Synth.* **1946**, *2*, 1–4.

(42) Si, S.; Bhattacharjee, R. R.; Banerjee, A.; Mandal, T. K. *Chem.—Eur. J.* **2006**, *12*, 1256–1265.
(43) Reches, M.; Gazit, E. *Nano Lett.* **2004**, *4*, 581–585.
(44) Ray, S.; Haldar, D.; Drew, M. G. B.; Banerjee, A. *Org. Lett.* **2004**, *6*, 4463–4465.
(45) Bodanszky, M.; Bodanzsky, A. In *The Practice of Peptide Synthesis*; Springer-Verlag: New York, 1984; pp 1−282.
(46) Loschonsky, S.; Couet, J.; Biesalski, M. *Macromol. Rapid Commun.* **2008**, *29*, 309–315.
(47) Robinson, K. L.; Khan, M. A.; de Paz Banez, M. V.; Wang, X. S.; Armes, S. P. *Macromolecules* **2001**, *34*, 3155–3158.
(48) Haddleton, D. M.; Heming, A. M.; Kukulj, D.; Duncalf, D. J.; Shooter, A. J. *Macromolecules* **1998**, *31*, 2016–2018.
(49) Garcia, M. F.; de la Fuente, J. L.; Fernandez-Sanz, M.; Madruga, E. L. *Polymer* **2001**, *42*, 9405–9412.
(50) Teodorescu, M.; Matyjaszewski, K. *Macromolecules* **1999**, *32*, 4826–4831.
(51) Teodorescu, M.; Matyjaszewski, K. *Macromol. Rapid Commun.* **2000**, *21*, 190–194.
(52) Adams, D. J.; Young, I. *J. Polym. Sci., Part A: Polym. Chem.* **2008**, *46*, 6082–6090.
(53) Chatterjee, D. P.; Chatterjee, U.; Mandal, B. M. *J. Polym. Sci., Part A: Polym. Chem.* **2004**, *42*, 4132–4142.
(54) Erhardt, R.; Boker, A.; Zettl, H.; Kaya, H.; Pyckhout-Hintzen, W.; Krausch, G.; Abetz, V.; Muller, A. H. E. *Macromolecules* **2001**, *34*, 1069–1075.
(55) Erhardt, R.; Zhang, M. F.; Boker, A.; Zettl, H.; Abetz, C.; Frederik, P.; Krausch, G.; Abetz, V.; Muller, A. H. E. *J. Am. Chem. Soc.* **2003**, *125*, 3260–3267.
(56) Hong, H.; Mai, Y.; Zhou, Y.; Yan, D.; Cui, J. *Macromol. Rapid Commun.* **2007**, *28*, 591–596.
(57) Zhang, L.; Eisenberg, A. *J. Am. Chem. Soc.* **1996**, *118*, 3168–3181.
(58) Yu, K.; Eisenberg, A. *Macromolecules* **1996**, *29*, 6359–6361.